Design of equidistant and revert type precipitation patterns in reaction–diffusion systems†

Ferenc Molnár Jr,[a] Ferenc Izsák[bc] and István Lagzi*[ad]

Received 12th October 2007, Accepted 13th February 2008
First published as an Advance Article on the web 6th March 2008
DOI: 10.1039/b715775d

In the past years considerable attention has been devoted to designing and controlling patterns at the microscale using bottom-up self-assembling techniques. The precipitation process proved itself to be a good candidate for building complex structures. Therefore, the techniques and ideas to control the precipitation processes in space and in time play an important role. We present here a simple and technologically applicable technique to produce arbitrarily shaped precipitation (Liesegang) patterns. The precipitation process is modelled using a sol coagulation model, in which the precipitation occurs if the concentration of the intermediate species (sol) produced from the initially separated reactants (inner and outer electrolytes) reaches the coagulation threshold. Spatial and/or temporal variation of this threshold can result in equidistant and revert (inverse) type patterns in contrast to regular precipitation patterns, where during the pattern formation a constant coagulation threshold is supposed and applied in the simulations. In real systems, this threshold value may be controlled by parameters which directly affect it (*e.g.* temperature, light intensity or ionic strength).

Introduction

Several pattern formation phenomena can be observed in organic and inorganic systems governed by reaction and diffusion (skin patterns, growth of bacterial colonies; rock patterns or periodic precipitation).[1] Pattern formation mechanisms and the corresponding mathematical models are different in general. However, these structures can be grouped as steady or unsteady (spatial behaviour) and static or dynamic (temporal behaviour) as well. Most of them often emerge in the wake of a moving reaction front. A well-known and spectacular example of these patterns is the Liesegang phenomenon.[2] In this case, the quasi-periodic pattern occurs due to a precipitation reaction between certain chemical species, one of them diffuses into a gel (outer electrolyte) and another one is homogeneously distributed in the gel matrix (inner electrolyte). The produced pattern consists of a set of precipitation bands or rings (depending on the geometry of the system), which are perpendicular to the diffusion flux of the invading (outer) electrolyte.

The precipitation pattern formation phenomena have been studied for 110 years,[2] nevertheless the experimental and theoretical investigations are still in the focus of researchers from different fields.[3–13] Recent interest in these structures originated from the possibility of designing and controlling microscopic patterns. Using the wet stamping technique (WETS—developed at Northwestern University) material deposition in porous media and spatially controlled pattern formation can be achieved.[14] Nevertheless, several interesting open questions are still under discussion: explanation and mathematical modelling of precipitation spiral (helical formation of precipitate),[15] revert (inverse) type[16–22] and tubular pattern formation in 3D.[23–25]

Detailed studies on the classical Liesegang patterns have shown four basic empirical laws,[26–31] in which the following macroscopic quantities of the pattern structure and evolution are connected with each other: x_n, the position of the nth precipitation zone measured from the junction point of electrolytes; w_n, the width of the nth band; and t_n, the time elapsed until its formation. The most important of them are the spacing and time laws. The spacing law[26] states that the positions of the precipitate zones approximate a geometrical series where $1 + p$ is the spacing coefficient:

$$\lim_{n\to\infty} \frac{x_{n+1}}{x_n} = 1 + p,\ p > 0. \quad (1)$$

This means that the bands are not equidistant. According to the time law[27] the position of the nth zone is linearly proportional to the square root of time elapsed until its formation:

$$x_n \sim \sqrt{t_n}. \quad (2)$$

This reflects the fact that the governing force of the pattern formation is the diffusion flux of the invading (outer) electrolyte, the concentration of which is 1–2 orders of magnitude higher than that of the inner one in a usual experimental setup.

[a] *Eötvös University, Institute of Chemistry, H-1117, Pázmány sétány 1/A, Budapest, Hungary. E-mail: lagzi@vuk.chem.elte.hu; Fax: +36 (06)1209 0555; Tel: +36 (06)1209 0555*
[b] *Eötvös University, Department of Applied Analysis and Computational Mathematics, H-1117, Pázmány sétány 1/C, Budapest, Hungary. Fax: +36 (06)1381 2158; Tel: +36 (06)1381 2157*
[c] *Twente University, EWI NACM, P.O. Box 217, 7500 AE Enschede, the Netherlands. Fax: +31 (0)534894833; Tel: +31 (0)534893408*
[d] *Eötvös University, Department of Meteorology, Budapest, Hungary. Fax: +36 (06)1372 2904; Tel: +36 (06)1372 2945*

† Electronic supplementary information (ESI) available: ES1 is the simulation program written for the Windows platform which shows the evolution of the precipitation (Liesegang) pattern in the case of constant coagulation threshold. ES2 is the simulation program written for the Windows platform which shows the evolution of the precipitation pattern when the coagulation threshold is homogeneously decreased producing an equidistant pattern structure. See DOI: 10.1039/b715775d

This pattern formation is usually explained with two different models: in the first one the outer and inner reactants turn directly into precipitate (A + B → P), whenever their local concentration product is above a given threshold value (solubility product).[32–35] In the second one the existence of an intermediate species C is assumed according to the reactions A + B → C → P.[36,37] The C particles are produced in a moving reaction front and the precipitation process takes place only if the local concentration of C reaches some threshold c^* (coagulation threshold value).

Motivation

It has been supposed in all models ever developed to describe pattern formation phenomena that the given threshold values are constant in space and time in order that the produced bands (zones, rings) may satisfy the existing regularities.[38–50] Constant threshold values also require that the spatial distribution of the pattern be quasiperiodic. Therefore, an appropriate temporal and/or spatial control of the coagulation threshold can result in different types of patterns compared to classical and regular ones. On the other hand, investigation and understanding of the control mechanism of pattern formation is the most important element for designing applicable micropatterns.

In this paper, we show that the systematic control of coagulation threshold can produce equidistant precipitation structures and even revert (inverse) type Liesegang patterns in a pure diffusion system.

Model

To illustrate our idea, we have chosen a simple precipitation mechanism (2:1 type, A_2B; P corresponds to the most common type of precipitate, *e.g.* $Ag_2Cr_2O_7$, PbI_2), giving rise to precipitation patterns, according to the reactions:

$$2A + B \rightarrow C, \tag{3}$$

$$C + P \rightarrow 2P. \tag{4}$$

Here A and B denote the outer and the inner electrolytes respectively, while C and P denote the intermediate species and the precipitation product, respectively. In a 1D setup, the governing equations corresponding to eqn (3)–(4) are given as a system of partial differential equations

$$\frac{\partial a}{\partial t} = D_a \frac{\partial^2 a}{\partial x^2} - 2ka^2b, \tag{5}$$

$$\frac{\partial b}{\partial t} = D_b \frac{\partial^2 b}{\partial x^2} - ka^2b, \tag{6}$$

$$\frac{\partial c}{\partial t} = D_c \frac{\partial^2 c}{\partial x^2} + ka^2b - \kappa_1 c\Theta(c - c^*) - \kappa_2 cp, \tag{7}$$

$$\frac{\partial p}{\partial t} = \kappa_1 c\Theta(c - c^*) + \kappa_2 cp, \tag{8}$$

for $t \in (t_0, T)$ and $x \in (0, X)$. Here a, b and c yield the concentrations of A, B and C respectively, while p yields the amount of the precipitate. D_a, D_b, and D_c are the diffusion coefficients of the corresponding species. k is the chemical rate constant for eqn (3), and κ_1, κ_2 are the rate constants for the coagulation and the autocatalytic precipitate formation, respectively. Θ denotes the Heaviside step function. In the simulations, the following initial conditions were used:

$$a(t_0,x) = a_0\Theta(x_{gel} - x), \tag{9}$$

$$b(t_0,x) = b_0\Theta(x - x_{gel}), \tag{10}$$

$$c(t_0,x) = 0, \tag{11}$$

$$p(t_0,x) = 0, \tag{12}$$

where x_{gel} is the position of the junction point of the electrolytes ($x_{gel} = 1.8$ cm) and $t_0 = 0$ is the initial time. Eqn (5)–(8) have been solved using a standard "method of lines" technique. Spatially a standard finite-difference method on a 1D equidistant grid was applied followed by time integration to solve the resulting ordinary differential equations with the following boundary conditions:

$$a|_{x=0} = a_0, \tag{13}$$

$$\left.\frac{\partial b}{\partial x}\right|_{x=0} = \left.\frac{\partial c}{\partial x}\right|_{x=0} = \left.\frac{\partial a}{\partial x}\right|_{x=X} = \left.\frac{\partial b}{\partial x}\right|_{x=X} = \left.\frac{\partial c}{\partial x}\right|_{x=X} = 0. \tag{14}$$

The length of the reaction medium is 18 cm. Usually, the concentration of A is kept fixed during the reaction, which corresponds to the boundary condition (13). For the species A at other part of the boundary and the other species at each part of the boundary a homogeneous Neumann-type boundary condition has been applied *cf.* eqn (14). Table 1 shows the parameters and constants used in the calculations.

Method

The main idea of a coagulation and precipitate growth model is that coagulation of the intermediate species (C) occurs when the local concentration reaches the coagulation threshold c^* [expressed as $\kappa_1 c\Theta(c - c^*)$]. This step corresponds to homogeneous nucleation, which can be modelled by a first order reaction. Wherever some precipitate exists, species C also reacts with P producing more precipitate (*cf.* with $\kappa_2 cp$). This process (precipitate or crystal growth) is expressed by quadratic autocatalytic reaction, because presence of some precipitate accelerates its formation. The above two terms in eqn (7)–(8) correspond to homogeneous nucleation and after that an autocatalytic precipitate growth occurs.[41] We have varied the coagulation threshold either spatially [$c^* = c^*(x)$] or temporally [$c^* = c^*(t)$] in such a way that the bands are formed at predetermined positions.

Table 1 Parameter set used in the model simulations (Δx and Δt are the grid spacing and time step respectively)

Δx	Δt	k	κ_1	κ_2	a_0	b_0	D_a	D_b	D_c
10^{-4} m	2.5 s	1 L^2 s^{-1} mol^{-2}	10^{-2} s^{-1}	1 L s^{-1} mol^{-1}	0.34 mol L^{-1}	0.036 mol L^{-1}	10^{-9} m^2/s	10^{-9} m^2/s	10^{-11} m^2/s

Results and discussion

The design procedure of the equidistant precipitation structures consists of four consecutive parts.

(i) Determination of the wavelength for the equidistant pattern.

First, one must choose the wavelength for the equidistant pattern that defines the distance between two precipitation bands. This way, we will have the explicit locations (measured from the junction point of the electrolytes) where we want the bands to appear.

(ii) Determination of the coagulation threshold for the equidistant pattern.

We determine the coagulation threshold (both in space and time) from a simulation, where we detect the motion of the intermediate product's concentration peak without any precipitation processes ($c^* \rightarrow \infty$) in such a way that a precipitation band formation is artificially provoked at the interface at the beginning of the diffusion process. The moving peak value is stored at the prescribed, user-defined locations for the equidistant pattern. This maximum exists since it has an approximately Gaussian distribution. The movement of the distribution and the peak is driven by two processes: the intermediate product is formed by the moving reaction front and consumed by the autocatalytic growth of the previous band. At the prescribed locations (where the bands should exist), precipitation is again artificially provoked such that c^* is set to the given Gaussian peak value.

(iii) Determination of the continuous coagulation limit function by fitting for time- or space-dependent individual thresholds.

After the simulation, the individual coagulation values (either in space or time) are recorded and continuous functions (coagulation limit functions) are fitted to the observed peak values. Instead of high order polynomial functions we have chosen exponential coagulation limit functions:

$$c^*(x) = c_{x0} + A_x \exp(x/\alpha), \quad (15)$$

$$c^*(t) = c_{t0} + A_t \exp(t/\beta), \quad (16)$$

which provide an accurate fitting using only three parameters c_{x0}, A_x, α and c_{t0}, A_t, β respectively. In the case of many physical processes either linear or exponential variation of some quantities (such as temperature or light intensity) result in an exponential change of those coefficients which describe the process (coagulation threshold, reaction rate coefficients). Therefore, natural processes (*e.g.* homogeneous cooling) are candidates for generating equidistant patterns either in the laboratory or in nature.

(iv) Simulation using fitted threshold function to obtain 'designed' equidistant pattern.

After fitting using this continuous threshold function a new simulation can be performed with the same parameter set. The resulting pattern structure may substantially differ from the regular and classical ones. During the simulation, the coagulation threshold varies in contrast to the 'classical' situations, where this value is taken as constant and a regular Liesegang pattern is produced.

Fig. 1 shows the fitted coagulation threshold functions in the case of different equidistant patterns characterized by individually determined wavelengths (λ). If the coagulation limit is above the corresponding value of the coagulation limit function [in space and time; eqn (15) and (16)], one can detect a diverging (Liesegang-like) pattern structure (Fig. 2a). In contrast to this situation, an equidistant pattern can be generated using the spatially or temporally varied coagulation limit functions determined from the simulation described above (Fig. 1). Fig. 2b and 2c represent the equidistant patterns designed using these continuous functions. In Fig. 2b, one can see that the coagulation threshold is stationary and spatially inhomogeneous. Apart from the first few bands (related to a transient period) the generated pattern is equidistant. Similar behaviour can be observed when c^* is a decreasing function of time (spatially homogenous and time-dependent coagulation threshold; *e.g.* homogeneous cooling, Fig. 2c). In general, the growth rate of the governing peak (the nearest one to the reaction front), monotonically decreases before it reaches the coagulation threshold, due to the diffusive behaviour of the reacting species. This involves the new precipitation bands forming further and further from each

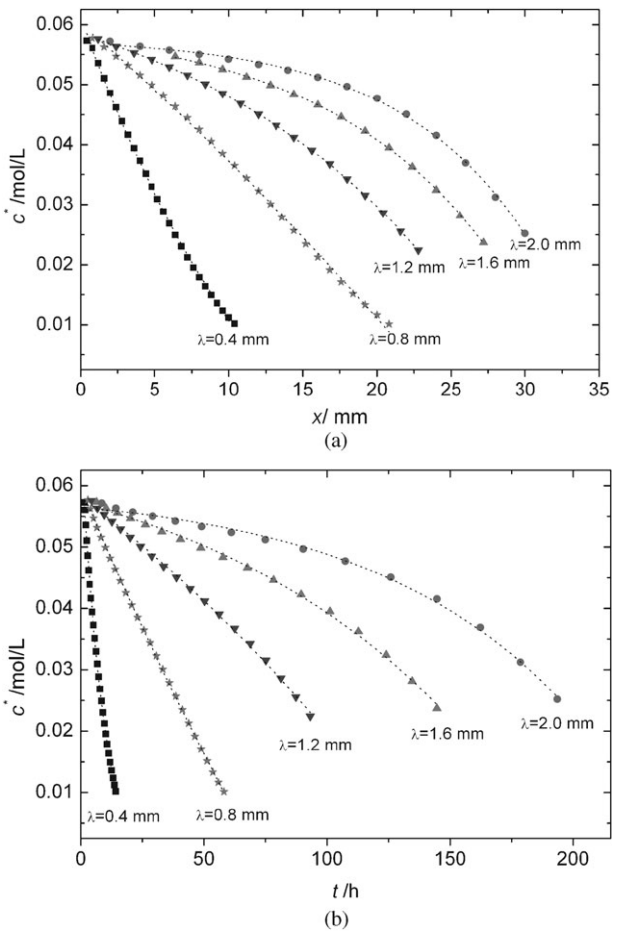

Fig. 1 Coagulation threshold functions at different wavelengths (λ) prescribed for the equidistant precipitation patterns when the variations are (a) stationary but spatially inhomogeneous and (b) spatially homogeneous but changing in time. The dotted lines correspond to the fitted exponentially deceasing functions.

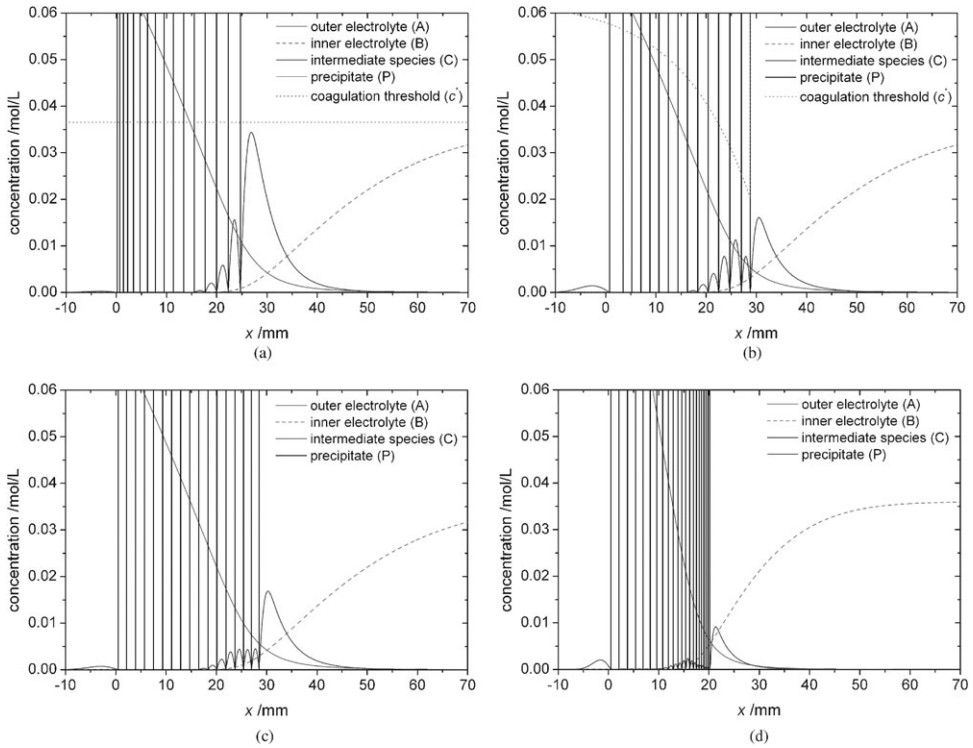

Fig. 2 Spatial distribution of the intermediate species, precipitate and the outer and inner electrolytes respectively at $t = 168.00$ h. Images show the following cases: (a) diverging Liesegang-like pattern where the coagulation threshold is a function of time, decreasing slower than prescribed for an equidistant pattern ($c_{t0} = 0.06931$ mol/L, $A_t = -0.01215$ mol/L and $\beta = 397\,949$ s); (b) equidistant pattern with 1.6 mm wavelength, created by a spatially inhomogeneous coagulation threshold ($c_{x0} = 0.06302$ mol/L, $A_x = -0.00512$ mol/L and $\alpha = 0.01351$ m); (c) equidistant pattern with 1.6 mm wavelength, created by a time-dependent coagulation threshold, ($c_{t0} = 0.06931$ mol/L, $A_t = -0.01215$ mol/L and $\beta = 397\,949$ s); (d) revert-type pattern where the coagulation threshold is a function of time, decreasing faster than prescribed for an equidistant pattern ($c_{t0} = 0.06931$ mol/L, $A_t = -0.01215$ mol/L and $\beta = 397949$ s).

other. If the coagulation threshold is decreased, the new bands will be formed closer to each other. Therefore, both equidistant and arbitrarily spaced patterns can be generated by controlling c^*. The results of equidistant pattern generation are shown in Fig. 3. The linear dependence between the band number and the position of the bands suggests that an equidistant pattern can be generated in contrast to the classical Liesegang experimental situation, where the coagulation limit cannot be changed (Fig. 3a).

The main advantage of this idea is that patterns of arbitrary shape can be designed and formed. Arbitrary shape means that the classical, equidistant or revert spaced pattern can be generated with this idea. The Matalon–Packter law states that the spacing coefficient in eqn (1) for classical patterns depends on the concentration of the electrolytes in a non-linear way.[31] Until now, this law suggested only a limited way to control the regular pattern structure (where the spacing between two bands is increased) *via* variation of the outer and inner electrolyte concentrations.[31] However, variation and control of the coagulation threshold represents a general way to design regular, revert and, in specialized cases, equidistant precipitation patterns. It is easily understandable: if the coagulation threshold is lower than the ones used in equidistant pattern generation (Fig. 1a and b) in every time and space position, the bands will be formed closer and closer to each other (Fig. 2d) in contrast to the regular Liesegang patterns.[16–22] This so-called revert (inverse) type pattern has been known for a long time in AgI system but its evolution has not yet been modeled.[16,17,21,22] The explanation of the revert spaced pattern has been based on ion adsorption on the precipitated silver iodide and flocculation.[21,22] Other Liesegang systems ($PbCr_2O_7$, $PbCrO_4$, $CuCrO_4$ and $Fe_3[Fe(CN)_6]_2$) are known to exhibit similar behaviour.[22] Fig. 4 depicts an experimentally observed revert Liesegang pattern in a silver iodide system in gelatine gel using classical Liesegang experimental setup, and here the revert type of pattern evolves spontaneously. Our simulations suggest a possible explanation of such pattern formation, namely that the coagulation threshold could simultaneously vary in space and time due to the special character of the silver iodide sol. The description of the revert type pattern formation could be the following: the formed silver iodide sol can adsorb silver ions on its surface. Therefore, a charged double layer is formed, which is very stable because the silver ion prefers to adsorb on sol surface producing stable particles. An electrostatic double layer prevents the coagulation, but after some time, this positively charged layer can be neutralized by adsorption of nitrate ions. Neutralization means that the sol particles can coagulate producing precipitate. From the mathematical point of view, this neutralization can be interpreted by the continuous decrease of the coagulation threshold. In conclusion, a reasonable explanation of revert pattern

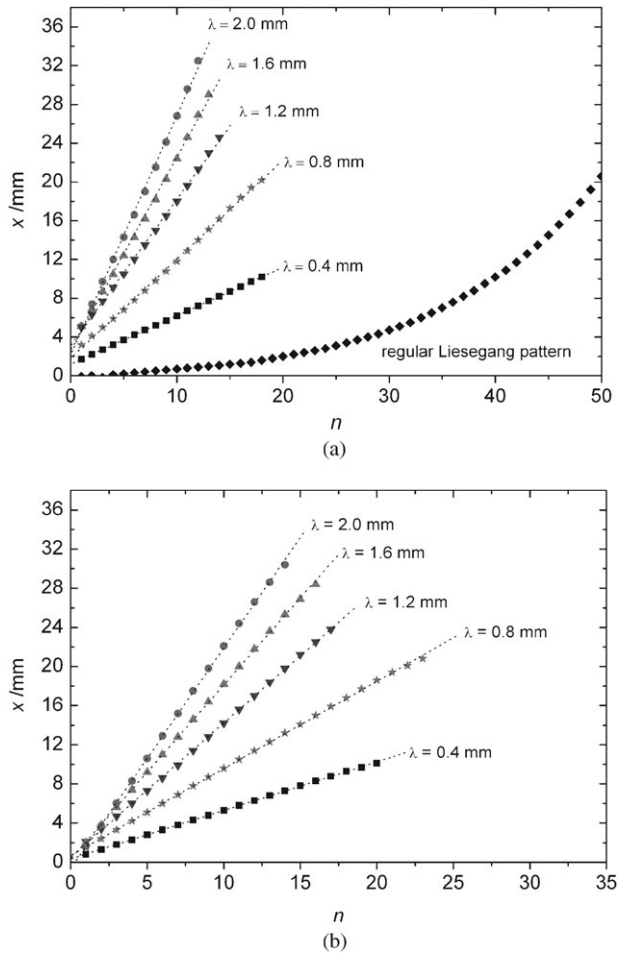

Fig. 3 Band position measured from the junction point of the electrolytes *versus* its band number at different wavelength (λ) of precipitation patterns, where the coagulation threshold was (a) stationary but spatially inhomogeneous, and (b) spatially homogeneously varied. Linear dependence suggests and demonstrates that the designed patterns are equidistant.

formation in thermostatic conditions could be that the coagulation threshold is varied either spatially or temporally due to the variation of the sol stability.

Conclusions

We have provided a simple and general method to modify and control the precipitation pattern in reaction–diffusion systems. The main advantage of the method described in this article is that arbitrary patterns can be generated in pure diffusion systems without any external forces as advection[51] or ionic migration.[52,53] Equidistant pattern can be formed only in a case when the coagulation threshold coincides with the corresponding value of the coagulation limit function. Taking smaller threshold values in every position at any time results in inverse type pattern, while higher ones result in Liesegang-like (diverging) precipitation structures. The coagulation threshold cannot be directly changed; it is coupled to control parameters, *e.g.* temperature and light intensity. It is known that temperature affects the coagulation concentration, and in a special precipitation system (lead chromate) the precipitation

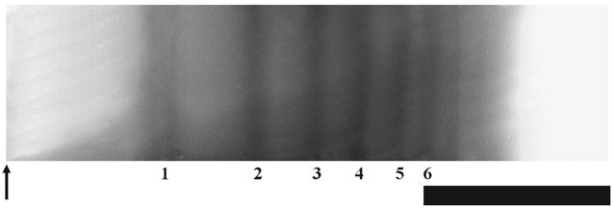

Fig. 4 The revert (inverse) AgI precipitation pattern in gelatine gel (16%) after 3 weeks. The distance between two consecutive bands is decreasing, which is in contrast to the regular Liesegang phenomenon, where it must be increasing. The concentration of the outer ($AgNO_3$) and inner (KI) electrolytes were 0.4 and 0.04 M, respectively. The arrow indicates the junction point of the outer and inner electrolytes. The scale bar represents 1 cm.

process strongly depends on light intensity: in the absence of illumination precipitation and pattern formation do not occur.[54] This suggests that if the relation between the coagulation limit and the control parameter is known and explored, the systematic variation of the control parameter can be used to design arbitrary patterns. Recently, it has been presented that a simple guiding field is sufficient to generate crossover between regular and inverse patterns using spinodal decomposition scenario for precipitate formation.[55]

We pointed out two very important findings. At first, one possible relevant interpretation of revert or irregular precipitation pattern structures in nature could be explained by the fact that in these systems this governing coagulation threshold may vary spatially and/or temporally. In nature there is no indication that this limit should be constant compared to experiments in thermostatic conditions. The coagulation threshold itself may depend on the chemical and physical properties of the system. Therefore classical regular patterns cannot be expected in all cases.

Secondly, from the technological point of view, the most important thing is how we can design and control microscopic or even nanosize patterns on material surfaces or in porous media. One should prepare surfaces and porous media by prescribed methods in a way that it indirectly controls the coagulation threshold. The choice of such techniques is the hardest task from the experimental point of view. Materials and methods affecting the adsorbility of sol particles could be candidates for the change and control of the coagulation threshold (*e.g.* pattern formation of silver particles from silver ions in glass[56]). The knowledge of the system, which includes information on the relation between the control parameter and the coagulation threshold value is the key element for designing micropatterns using the technique described here.

Acknowledgements

The authors gratefully acknowledge financial support from the Hungarian Scientific Research Found (OTKA D048673 and OTKA K68253), the Öveges Research Fellowship from the Hungarian National Office for Research and Technology and Bolyai Research Fellowship of the Hungarian Academy of Sciences.

References

1 B. A. Grzybowski, K. J. M. Bishop, C. J. Campbell, M. Fialkowski and S. K. Smoukov, *Soft Matter*, 2005, **1**, 114.
2 R. E. Liesegang, *Naturwiss. Wochenschr.*, 1896, **11**, 353.
3 J. Maselko, P. Borisova, M. Carnahan, E. Dreyer, R. Devon, M. Schmoll and D. Douthat, *J. Mater. Sci.*, 2005, **40**, 4671.
4 J. Maselko, A. Geldenhuys, J. Miller and D. Atwood, *Chem. Phys. Lett.*, 2005, **373**, 563.
5 J. George and G. Varghese, *J. Colloid Interface Sci.*, 2005, **282**, 397.
6 M. I. Lebedeva, D. G. Vlachos and M. Tsapatsis, *Phys. Rev. Lett.*, 2004, **92**, 883011.
7 M. I. Lebedeva, D. G. Vlachos and M. Tsapatsis, *Ind. Eng. Chem. Res.*, 2004, **43**, 3073.
8 Y. I. Sukharev and B. A. Markov, *Mol. Phys.*, 2004, **102**, 745.
9 F. Arteaga-Larios, E. Y. Sheu and E. Perez, *Energ. Fuel.*, 2004, **18**, 1324.
10 A. Toramaru, T. Harada and T. Okamura, *Phys. D*, 2003, **183**, 133.
11 I. Das and A. Bajpai, *J. Sci. Ind. Res.*, 2001, **60**, 10.
12 V. V. Kravchenko, A. B. Medvinskii, V. I. Emelyanenko, A. N. Reshetilov and G. R. Ivanitskii, *Biofizika*, 2000, **45**, 102.
13 D. Xie, J. Wu, G. Xu, Q. Ouyang, R. D. Soloway and T. Hu, *J. Phys. Chem. B*, 1999, **103**, 8602.
14 B. A. Grzybowski and C. J. Campbell, *Mater. Today*, 2007, **10**, 38.
15 Daishin Ueyama, private communication (Meiji University), 2007.
16 N. Kanniah, F. D. Gnanam and P. Ramasamy, *J. Colloid Interface Sci.*, 1983, **94**, 412.
17 N. Kanniah, F. D. Gnanam, P. Ramasamy and G. S. Laddha, *J. Colloid Interface Sci.*, 1981, **80**, 369.
18 P. B. Mathur and S. Ghosh, *Kolloid-Zeitschrift*, 1958, **159**, 142.
19 B. M. Metha and K. Kant, *Kolloid-Zeitschrift*, 1966, **209**, 54.
20 C. Rodriguez-Navarro, O. Cazalla, K. Elert and E. Sebastian, *P. Roy. Soc. A-Math. Phy.*, 2002, **458**, 2261.
21 N. Kanniah, F. D. Gnanam and P. Ramasamy, *Proc. Ind. Acad. Sci. (Chem. Sci.)*, 1984, **93**, 801.
22 M. Flicker and J. Ross, *J. Chem. Phys.*, 1974, **60**, 3458.
23 D. A. Stone and R. E. Goldstein, *Proc. Natl. Acad. Sci. U. S. A.*, 2004, **101**, 11537.
24 J. J. Pagano, S. Thouvenel-Romans and O. Steinbock, *Phys. Chem. Chem. Phys.*, 2007, **9**, 110.
25 S. Thouvenel-Romans, J. J. Pagano and O. Steinbock, *Phys. Chem. Chem. Phys.*, 2005, **7**, 2610.
26 K. Jablczynski, *Bull. Soc. Chim. Fr.*, 1923, **33**, 1592.
27 H. W. Morse and G. W. Pierce, *Proc. Am. Acad. Arts Sci.*, 1903, **38**, 625.
28 K. M. Pillai, V. K. Vaidyan and M. A. Ittyachan, *Colloid Polym. Sci.*, 1980, **258**, 831.
29 S. C. Müller, S. Kai and J. Ross, *J. Phys. Chem.*, 1982, **86**, 4078.
30 M. Droz, J. Magnin and M. Zrínyi, *J. Chem. Phys.*, 1999, **110**, 9618.
31 R. Matalon and A. Packter, *J. Colloid Sci.*, 1955, **10**, 46.
32 C. Wagner, *J. Colloid Sci.*, 1950, **5**, 85.
33 S. Prager, *J. Chem. Phys.*, 1956, **25**, 279.
34 Y. B. Zeldovitch, G. I. Barrenblatt and R. L. Salganik, *Sov. Phys. Dokl.*, 1962, **6**, 869.
35 D. A. Smith, *J. Chem. Phys.*, 1984, **81**, 3102.
36 G. T. Dee, *Phys. Rev. Lett.*, 1986, **57**, 275.
37 S. C. Müller and J. Ross, *J. Phys. Chem. A*, 2003, **107**, 7997.
38 M. Msharrafieh, M. Al-Ghoul, H. Batlouni and R. Sultan, *J. Phys. Chem. A*, 2007, **111**, 6967.
39 J. George and G. Varghese, *Chem. Phys. Lett.*, 2002, **362**, 8.
40 M. Chacron and I. L'Heureux, *Phys. Lett. A*, 1999, **70**, 263.
41 T. Antal, M. Droz, J. Magnin, Z. Rácz and M. Zrínyi, *J. Chem. Phys.*, 1998, **109**, 9479.
42 M. Al-Ghoul and R. Sultan, *J. Phys. Chem. A*, 2001, **105**, 8053.
43 Z. Rácz, *Phys. A*, 1999, **274**, 50.
44 T. Antal, M. Droz, J. Magnin and Z. Rácz, *Phys. Rev. Lett.*, 1999, **83**, 2880.
45 H.-J. Krug and H. Brandtstadter, *J. Phys. Chem. A*, 1999, **103**, 7811.
46 A. Büki, É. Kárpáti-Smidróczki and M. Zrínyi, *J. Chem. Phys.*, 1995, **103**, 10387.
47 A. A. Polezhaev and S. C. Müller, *Chaos*, 1994, **4**, 631.
48 M. E. LeVan and J. Ross, *J. Phys. Chem.*, 1987, **91**, 6300.
49 G. Venzl and J. Ross, *J. Chem. Phys.*, 1982, **77**, 1302.
50 J. B. Keller and S. I. Rubinow, *J. Chem. Phys.*, 1981, **74**, 5000.
51 F. Izsák and I. Lagzi, *J. Chem. Phys.*, 2005, **122**, 184707.
52 I. Bena, M. Droz and Z. Rácz, *J. Chem. Phys.*, 2005, **122**, 204502.
53 I. Lagzi, *Phys. Chem. Chem. Phys.*, 2002, **4**, 1268.
54 I. Das, R. S. Lall and A. Pushkarna, *J. Phys. Chem.*, 1987, **91**, 747.
55 T. Antal, I. Bena, M. Droz, K. Martens and Z. Rácz, *Phys. Rev. E*, 2007, **76**, 046203.
56 C. Mohr, M. Dubiel and H. Hofmeister, *J. Phys.: Condens. Matter*, 2001, **13**, 525.